Received 4 December 2023, accepted 29 December 2023, date of publication 5 January 2024, date of current version 12 January 2024.

Digital Object Identifier 10.1109/ACCESS.2024.3350194

RESEARCH ARTICLE

Interdimensional Interference Equalizing Using Recurrent Neural Network for Multi-Dimensional Optical Transmission

INHO HA, JOUNG-MOON LEE, JINWOO PARK, AND SANG-KOOK HAN, (Senior Member, IEEE)

Department of Electrical and Electronic Engineering, Yonsei University, Seodaemun-gu, Seoul 03722, South Korea

Corresponding author: Sang-Kook Han (skhan@yonsei.ac.kr)

This work was supported by the National Research Foundation of Korea (NRF) grant funded by the Korean Government, Ministry of Science and ICT (MSIT), through the Research on Machine Learning Based Multidimensional Optical Transmission for Intelligent Optical Access Network under Grant 2019R1A2C3007934.

ABSTRACT During multi-dimensional optical transmission, because of photodetector (PD) operation as a square law detector, signals get distorted when they are modulated on polarization and phase due to interdimensional interference (IDI) by intensity-modulated signals. We propose an IDI mitigation technique using recurrent neural network for multi-dimensional optical transmission. The signal transmission performance of the proposed equalization technique was experimentally analyzed. The performance of the proposed system was verified using the symbol error rate (SER).

INDEX TERMS Multi-dimensional optical modulation, interdimensional interference (IDI), recurrent neural network (RNN), optical access network.

I. INTRODUCTION

Recently, the use of various IoT and wearable devices has been increasing. Additionally, various applications targeting 5G and B5G have emerged. Therefore, high-capacity optical transmission is required for optical access networks, and it is essential to increase the transmission capacity of the optical transmission [1], [2], [3], [4]. Most of the techniques for high transmission capacity are affected by various factors, such as the fiber dispersion occurring during transmission, the frequency response of the devices, especially the physical limitation of the modulation bandwidth of the optical modulator, and limitations depending on the signal-to-noise ratio of the system [5], [6], [7], [8]. Therefore, several studies have been recently conducted on multi-dimensional transmission techniques by adding modulation resources to achieve high spectral efficiency and to eliminate these factors [9], [10], [11], [12]. We previously reported a single wavelength-based multi-dimensional optical transmission with a quadrature amplitude modulation-polarized intensity rotational frequency shift keying-differential phase shift keying (QAM-PIRFSK-DPSK) modulation technique, which is a novel multi-dimensional optical modulation technique [13], [14], [15], [16], [17], [18]. QAM-PIRFSK-DPSK modulation is more robust to changes in the state of polarization (SOP), especially the rotation SOP (RSOP), than polarization shift keying (PolSK)-based multi-dimensional optical modulation. In addition, because the QAM-PIRFSK-DPSK modulation is a multi-dimensional optical transmission based on direct detection, it is simpler than an optical coherent transmission system that requires a local oscillator (LO).

However, in multi-dimensional transmission has critical issues. In multi-dimensional optical transmission, interference occurs between signals modulated in other modulation dimensions. We refer to this as interdimensional interference (IDI). Because a photodetector (PD) is a square-law detector, it detects signals based on the intensity of the optical carrier. In other words, when a signal modulated in a dimension other than the intensity dimension is received, the IDI of the intensity dimension affects the signal. When a signal is received from the optical phase dimension, a signal modulated by the optical intensity dimension is received simultaneously.

The associate editor coordinating the review of this manuscript and approving it for publication was Ángel F. García-Fernández.

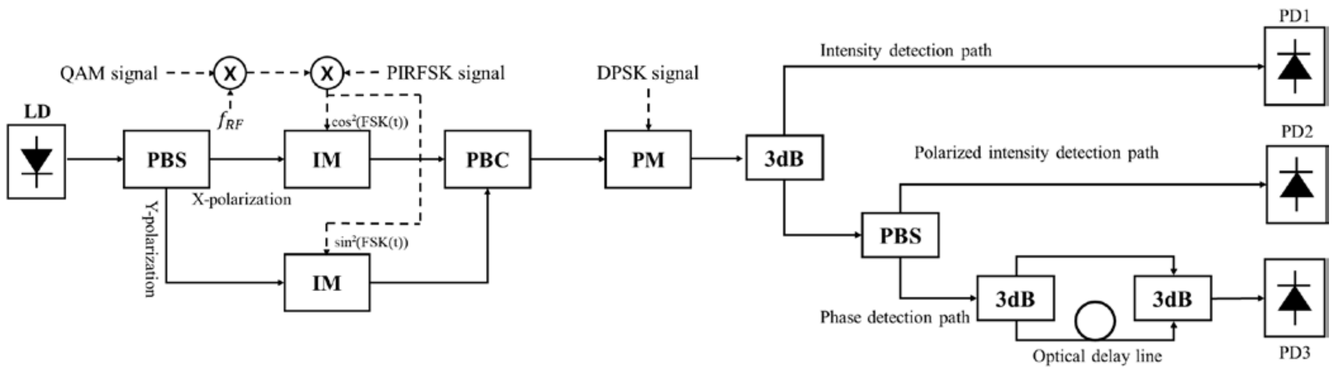

FIGURE 1. System schematic of QAM-PIRFSK-DPSK optical transmission.

The IDI from the optical-intensity dimension distorts the signal modulated by the phase dimension. In particular, in the case of a DPSK signal, because the delayed and original signals beat together to receive the phase signal, The IDI caused by the beating component of the delayed intensity signal and the original intensity signal affect the DPSK signal. Therefore, it is necessary to develop an IDI mitigation technique for signal detection modulated by phase dimensions.

In conventional studies on signal equalization, signal deterioration is compensated for by a linear equalizer. However, as the equalization performance deteriorates for complex degradations, research on nonlinear equalizers, such as the Volterra equalizer, was conducted [19], [19], [20], [21], [22]. Recently, performance improvement research has been conducted using artificial intelligence (AI)-based equalizers [23], [24], [25]. Conventional AI-based studies on optical access networks have mainly focused on classifiers; however, many studies on AI-based equalization have recently been conducted. The IDI generated during a multi-dimensional optical transmission is caused by various factors. An AI-based equalization technique is required to compensate for the signal deterioration caused by IDI.

In this study, we propose an interdimensional interference mitigation equalization technique using a recurrent neural network (RNN) for multi-dimensional optical transmission. For IDI using intensity modulated (IM) signals generated during DPSK signal detection, the multi-dimensional optical transmission performance was improved through RNN-based equalization. We theoretically and experimentally verified the performance of QAM-PIRFSK-DPSK transmission using symbol error rate (SER) analyses.

II. SCHEMATICS

We developed a system schematic for QAM-PIRFSK-DPSK optical transmission, as shown in Figure 1 [15]. In the proposed QAM-PIRFSK-DPSK modulation scheme, the PIRFSK and QAM signals are modulated in the optical intensity dimension, whereas the DPSK modulation is a signal modulated in the optical phase dimension. In the QAM-PIRFSK-DPSK system, the QAM and PIRFSK signals were modulated for each polarization of the optical carrier launched from the laser diode (LD) by intensity modulator (IM), like Mach-Zehnder modulator (MZM). The DPSK signal is modulated by the phase modulator (PM) to the optical carrier, which passes through the polarization beam combiner. The electrical fields of the modulated optical carrier are represented by Equations (1) – (7):

$$E_x = \sqrt{P}A_x(t)\exp\{-j(\omega t + S_{DPSK}(t))\}, \quad (1)$$
$$E_y = \sqrt{P}A_y(t)\exp\{-j(\omega t + S_{DPSK}(t) + \phi)\}, \quad (2)$$
$$A_x = \sqrt{S_{QAM}(t) + V_b} \times \cos(S_{FSK}(t)), \quad (3)$$
$$A_y = \sqrt{S_{QAM}(t) + V_b} \times \sin(S_{FSK}(t)), \quad (4)$$
$$S_{QAM}(t) = \alpha(t) \times \cos(2\pi f_{RF} t + \beta(t)), \quad (5)$$
$$S_{FSK}(t) = 2\pi f_i t, f_i = \{f_1, f_2, \ldots, f_m\}, \quad (6)$$
$$S_{DPSK}(t) = \varphi_i, \varphi_i = \{\varphi_1, \varphi_2, \ldots, \varphi_n\}. \quad (7)$$

The power of each polarization is set to P before the optical carrier passes through the polarization beam splitter. The phase difference between X and Y polarization of optical carrier is ϕ. Thereafter, a multi-dimensional optical signal is transmitted. After the multi-dimensional optical signal passes through the 3-dB coupler at the receiver, the QAM signal is received through the intensity of the optical carrier in Photodetector (PD)1. The PD is a square-law detector; therefore, signals are received at the PD based on the optical intensity. When a signal is received by PD1, signals other than QAM are not received [14], [15]. There was no effect on the IDI when the QAM signal was received.

The optical carrier passing through the 3-dB coupler was divided into polarizations through the PBS. Polarized optical carriers were received by PD2. The received signal at PD1 is the squared form of Equation (3). The multiplied result of QAM and PIRFSK signals was received. The PIRFSK signal did not change the amplitude and phase of the signal, and the QAM signal did not change its frequency. For PD2, the PIRFSK signal was affected by the IDI of the QAM signal; however, the effect was insignificant because it did not change the frequency.

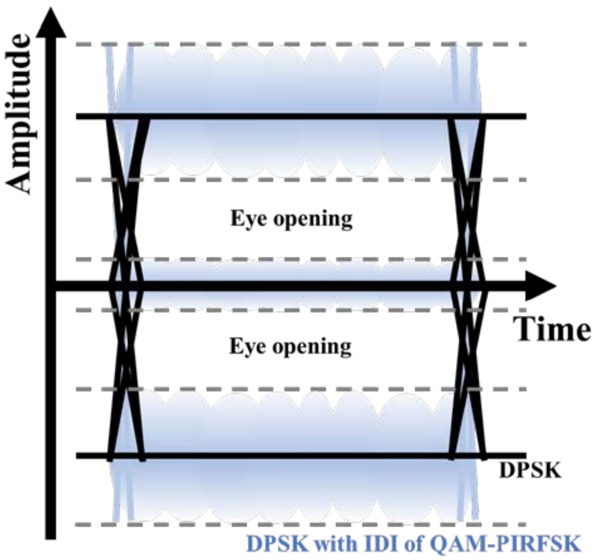

FIGURE 2. Eye diagram of DPSK signal with IDI and without IDI.

To receive the DPSK signal, the QAM and PIRFSK signals were simultaneously received. At this time, the QAM and PIRFSK signals deteriorated the DPSK signal performance. In particular, because the DPSK signal is received by beating between a delayed signal and a current signal through a Mach–Zehnder delay interferometer, the current and delayed QAM, PIRFSK, and DPSK signals are mixed, beat, and received. The phase detection path is shown in Figure 1. The signal was passed through a Mach–Zehnder delay interferometer (MZDI) including 3-dB couplers and an optical delay line. The signal passing through the MZDI was a combination of two signals. One is the original signal and the other is the delayed signal, which is delayed by one symbol period of the original signal. The two signals beat at PD3 during the signal reception. The equations for the signal received by PD3 are given by Equations (8) and (9).

$$\begin{aligned} E_{x\_n}(t) &= \frac{j}{2\sqrt{2}}\left[E_{x\_n}(t) - E_{x\_n-1}(t)\right] \\ &= \frac{j\sqrt{P}}{2\sqrt{2}}[A_{x\_n}(t)\exp\left\{-j\left(\omega t + S_{DPSK\_n}(t)\right)\right\} \\ &\quad - A_{x\_n-1}(t)\exp\left\{-j\left(\omega(t-T) + S_{DPSK\_n-1}(t)\right)\right\}] \end{aligned} \tag{8}$$

$$\begin{aligned} I_{PD3}(t) = \frac{1}{8}kRP\{&A_{x\_n}^2(t) + A_{x\_n-1}^2(t) \\ &+ 2A_{x\_n}A_{x\_n-1}\cos(S_{DPSK\_n}(t) - S_{DPSK\_n-1}(t))\} \end{aligned} \tag{9}$$

The DPSK signal was received using QAM and FSK signals. R is the responsivity of the photodiode, and k is the proportionality factor. A binary DPSK signal is received as a single-dimensional transmission is represented by the black line eye diagram in Figure 2. However, the DPSK signal received with the IDI of the QAM and PIRFSK signals is shown by the blue-line eye diagram in Figure 2. As mentioned above, the IDI that affects the DPSK signal is the beating value between the QAM, PIRFSK, and delayed signals at the PD. Because of these complex influences, AI-based equalization is required. As mentioned above, when receiving a DPSK signal in QAM-PIRFSK-DPSK, the performance degrades owing to the distortion by the QAM and PIRFSK signals modulated by the intensity of the optical carrier. In addition, because the signal passing through the MZDI was received, the original and delayed signals were mixed and received after beating at the PD. The data in the current state affect the next state.

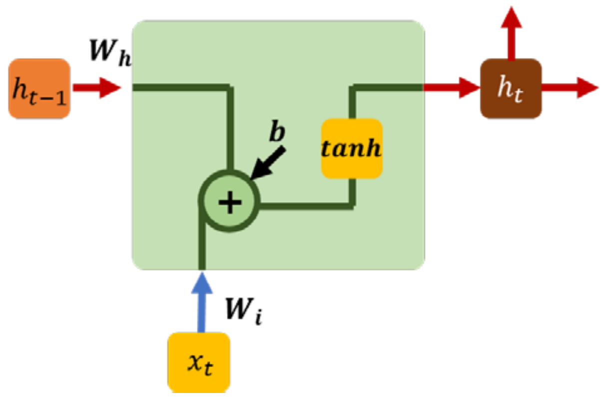

FIGURE 3. Concept of the Vanilla-RNN unit.

$$h_t = \tanh(W_h h_{t-1} + W_i x_t + b). \tag{10}$$

AI-based equalization with a recurrent structure was performed to input the delayed signal information. To equalize these IDI distortions, RNN-based equalization was performed in this study to improve performance. The RNN structure includes gated recurrent units (GRU), long short-term memory (LSTM), and vanilla units. The MZDI structure is identical to that of the vanilla RNN structure. Owing to the characteristics of the DPSK signal, the current signal affects only the next state; therefore, it does not match the LSTM and GRU signals that affect the later state. LSTM-based equalizers and GRU-based equalizers have higher complexity than vanilla RNN-based equalizers [25]. Additionally, since the IDI experienced in DPSK is only affected by the signal whose intensity has been modulated and the previous signal, the effect of long-term memory, which is an advantage of the LSTM-based equalizer, is minimal. In IDI, the influence between symbols only affects the symbol immediately following symbol. The impact of long-term memory is relatively reduced. Therefore, the GRU- and LSRM-based equalizer can compensate for the distorted signal caused by IDI as well as the vanilla RNN-based equalizer, but it is not suitable because it increases unnecessary complexity. In this paper, the performance of the proposed technique was verified through performance comparison with a 3rd-order

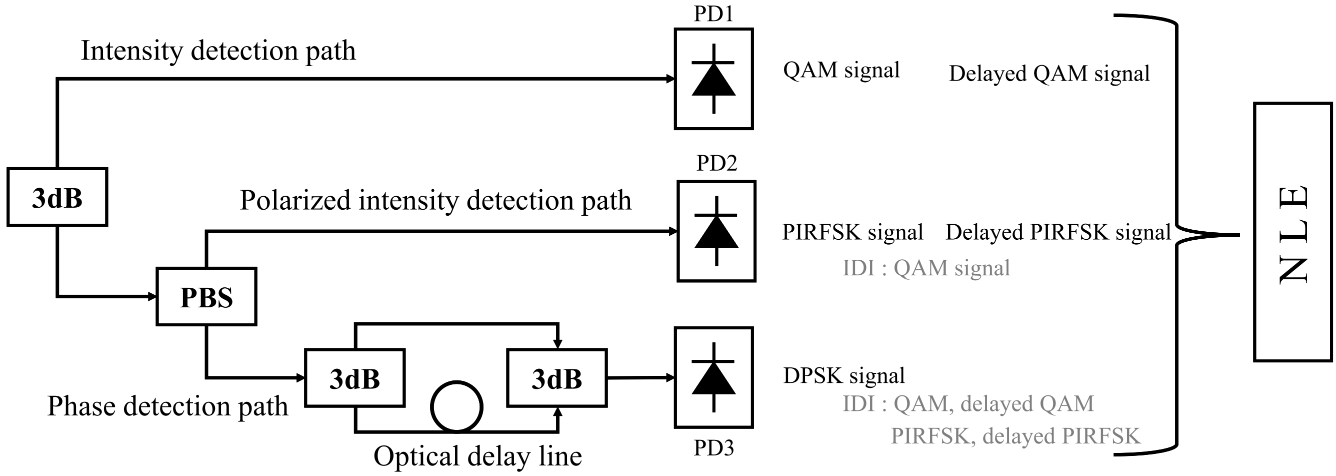

FIGURE 4. Receiver diagram for equalization of QAM-PIRFSK-DPSK transmission system.

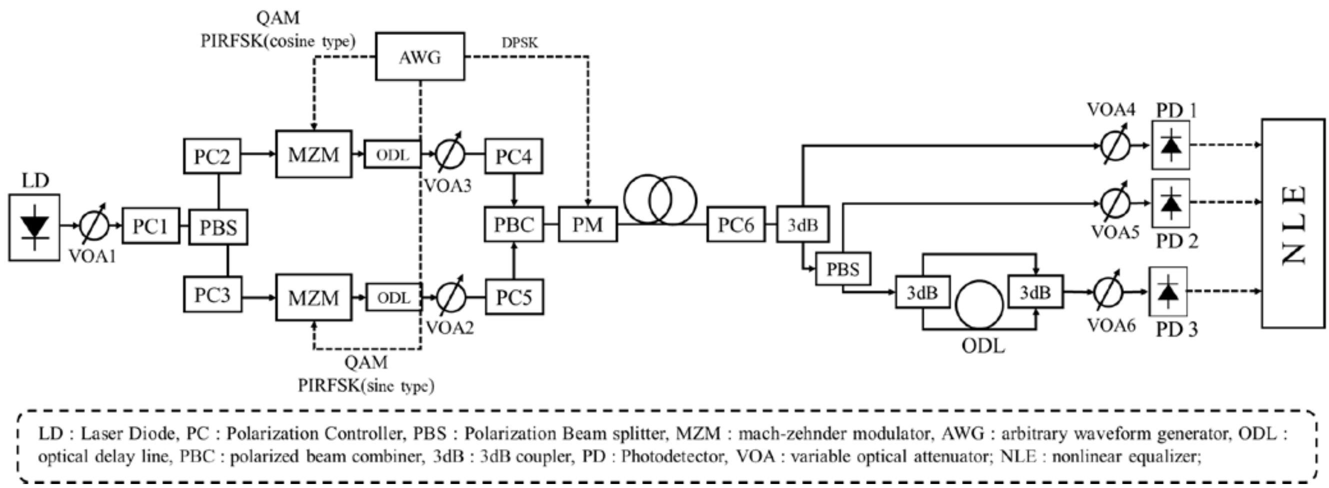

FIGURE 5. Experimental setup of QAM-PIRFSK-DPSK transmission system.

Volterra equalizer instead of an LSTM-based equalizer. As shown in Figure 3, the previous hidden output h_{t-1} of the previous state receives the weight W_h and enters with the x_t of the current input data, and tanh is the hyperbolic tangent activation function. We adopted the categorical cross-entropy loss function and ADAM optimizer as the cost function and optimization algorithm, respectively. Therefore, hidden output h_t is calculated using Equation (10). As shown in Figure 4, PD1 and PD2 receive the QAM and PIRFSK signals, respectively. Based on the received QAM and PIRFSK signals, the RNN equalizer learns from the DPSK signal received together with the IDI received from PD3. The amplitude of the IDI is affected by the modulation range of the MZM and QAM signals, and its frequency is influenced by the FSK signal. The RNN equalizer trains the QAM, delayed QAM, PIRFSK, delayed PIRFSK, and DSPK signals. The RNN equalization technique can mitigate the effects of interdimensional interference in a multi-dimensional QAM-PIRFSK-DPSK transmission system.

III. EXPERIMENTS AND RESULTS

Experiments were conducted to verify the performance enhancement of the proposed multi-dimensional optical transmission system. To test the proposed multi-dimensional optical transmission, an experiment was conducted, as shown in Figure 5. An external-cavity laser (ECL) diode was employed as the continuous wave (CW) laser source. The wavelength of the optical source was 1,550 nm. The optical power of the carrier was 12 dBm. Polarization controller (PC) 1 was used to divide the optical carriers from ECL into equal powers using polarization beam splitter (PBS). PC2 and PC3 were used to maximize the modulation performance of the MZMs. The QAM, PIRFSK, and DPSK signals were generated using an arbitrary waveform generator (AWG

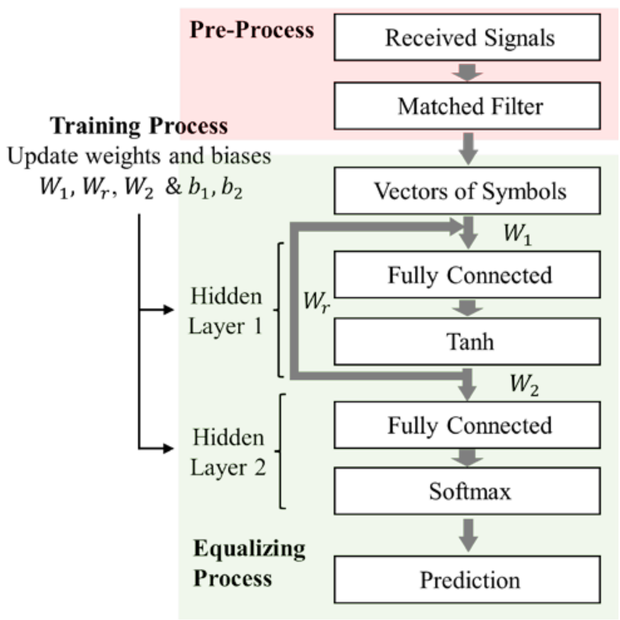

FIGURE 6. Schematic of RNN-based equalizer.

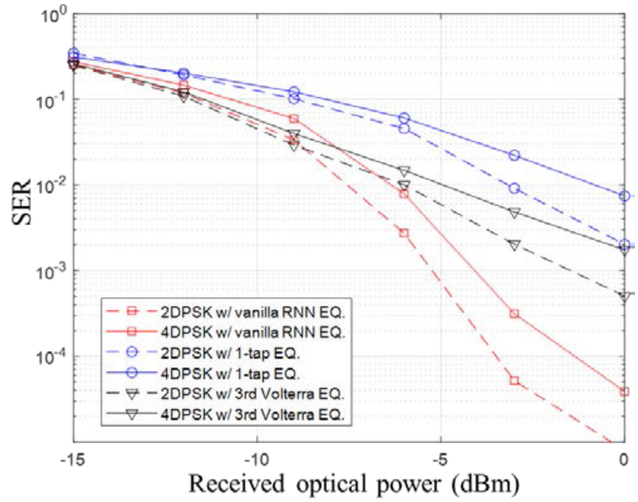

FIGURE 7. DPSK SER performance of the received 16QAM-Mary DPSK signal.

70002A; AWG). The vertical bit resolution of the AWG was 10 bits, and the sampling rate was set to 18 GHz. The QAM and PIRFSK signals were converted into optical signals by the intensity modulation of the optical carrier through two parallel MZMs. The signal multiplied by the QAM signal and the PIRFSK with a doubling frequency were modulated at the quadrature point (QP) of the MZMs. The modulation range of the modulator was set as 0.6. The modulated optical signals of the X- and Y-polarized optical carriers were synchronized using the optical delay line (ODL). Subsequently, the changed polarization states were made orthogonal to each other again through PC4 and PC5. The orthogonal polarized signals were combined using polarization beam combiner (PBC). The experiment was conducted using an optical transmission with a range of 20 km through a standard single-mode fiber (SSMF). The SOP of the signal was scrambled using PC6. As described above, the receiver includes three PDs to receive the signals modulated at each optical intensity, phase, and polarization. An unpolarized optical carrier is received at PD1. The polarized optical carrier that passed through the PBS was received at PD2. To construct the MZDI structure, we used a DPSK demodulator for the DPSK signal detection (Kylia; MINT 2.5 GHz). The DPSK signal is received at PD3 after the DPSK demodulator. The receiving sampling rate was set to 25 GHz at the digital storage oscilloscope (DSO). The received signal was stored using a DSO and offline processing was performed. The received signal was downsampled to 18 GHz using the DSP process.

The transmitted bits are generated using a pseudorandom binary sequence (PRBS). An electrical QAM signal with 1.25 GHz bandwidth and 16–64 QAM was upconverted to 1.25 GHz RF tone to modulate the optical carrier. The symbol rate of the QPSK signal was set 1.25 GBd. The PIRFSK signal was generated as a 2–4 FSK signal with a bit rate of approximately 1.25–2.5 Gbps, which is 1.25 GBd. The symbol period of the PIRFSK signal is maintained. The DPSK signal was transmitted signals as Mary-BPSK with a bit rate of approximately 2.5–5 Gbps, which is 2.5 GBd. Ten thousand symbols were generated and transmitted in each experiment. Signals were received at optical power between −15 and 0 dBm for each modulation.

In nonlinear equalization processing, we performed general signal demodulation and signal demodulation with RNN-based equalization. Offline DSP was conducted using the Keras library. We considered 3,000 data symbols for training and data 7,000 symbols for testing, using unknown data. Every symbol in each window contained five values as input (Figure 4), feeding the RNN layer of eight hidden units. The sequential neural model is illustrated in Figure 6. W_r is the recurrent weight, W_1 is the fully connected weight, and b_1 is the bias. W_2 is another fully connected weight, and b_2 is a different bias. Equations (11) and (12) show h_t and the output O_t.

$$h_t = \tanh(W_r h_{t-1} + W_1 x_t + b_1), \tag{11}$$
$$O_t = \mathrm{softmax}(W_2 h_t + b_2). \tag{12}$$

As shown above, the symbol duration of DPSK is half of those of QAM and PIRFSK. In other words, for the equalization of the DPSK signal, half the duration of the PIRFSK signal, half the duration of the QAM signal, half the duration of the delayed PIRFSK signal, and half the duration of the delayed QAM signal were used as training data along with the DPSK signal. An RNN equalizer was constructed based on the vanilla RNN model. A performance analysis was conducted according to the number of training sessions. After equalization, SER measurements were performed.

To measure the DPSK performance degradation caused by the IDI according to the expansion of the modulation

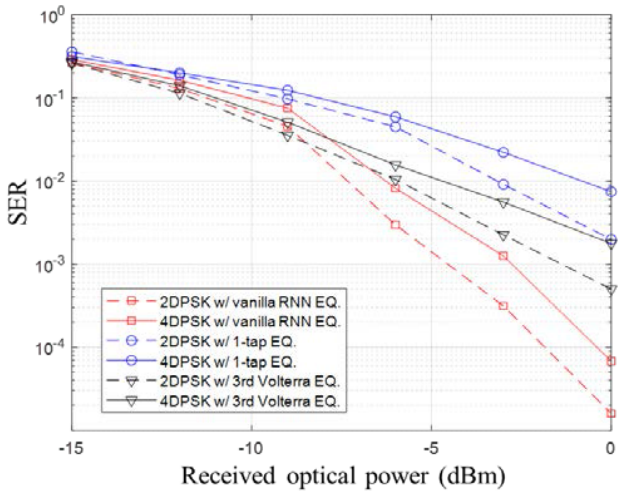

FIGURE 8. DPSK SER performance of the received 64QAM-PIR2FSK-Mary DPSK signal.

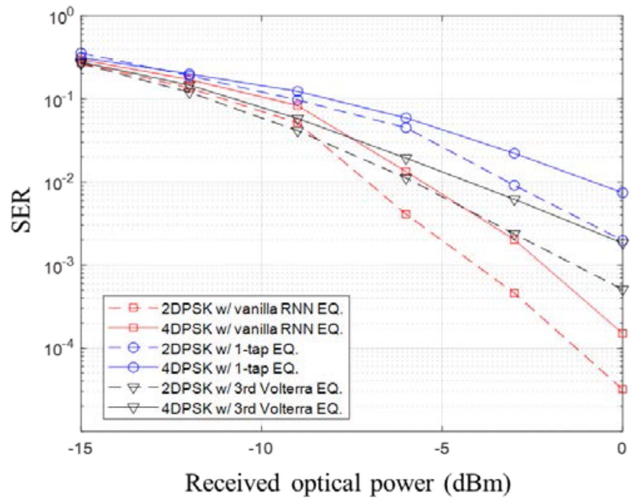

FIGURE 9. DPSK SER performance of the received 64QAM-PIR4FSK-Mary DPSK signal.

dimension in multi-dimensional optical transmission, the QAM and DPSK signals were modulated for 2-dimensional optical transmission. We compared the performance of the proposed RNN equalizer with a 1-tap linear equalizer and 3rd order Volterra equalizer to check the SER performance of the DPSK signal. Figure 7 shows the change in performance according to the DPSK modulation order during 2D transmission based on 16QAM. With 1-tap equalization, the 2DPSK signal exhibited an SER performance of less than 10^{-2} at -3 dBm optical power. The 4DPSK had an SER performance of 10^{-2} or less at -1 dBm or more. In addition, with 1-tap equalizer, the SER performance with increasing optical power did not significantly improve the SER performance. When a volterra equalizer is used, it has better SER performance than a 1-tap equalizer. However, like the 1-tap equalizer, using the volterra equalizer the SER performance with increasing optical power did not significantly improve the SER performance. However, after implementing the RNN-based equalization, the signal performance significantly improved. The 2DPSK has SER performance of 10^{-2} at -7.5 dBm. In particular, for 4DPSK, the SER graphs show considerable improvement, and the SER performance has 10^{-2} at about -6.4 dBm.

PIRFSK was simultaneously modulated to expand the modulation dimensions to three. Figure 8 shows the SER performance when a DPSK signal is received together with a 64QAM-PIR2FSK signal. Similar to the case of the 2D optical transmission shown in Figure 7, the performance of the DPSK signals significantly degraded with 1-tap equalizer and Volterra equalizer. After RNN-based equalizer, the SER performance of the DPSK signals improved significantly. Compared with 2D optical transmission, the performance decreased slightly. The IDI level increased with an increase in the modulation order of the QAM, and the IDI frequency also increased owing to the PIRFSK signal. As a result, the IDI performance improvement by RNN equalization was slightly reduced.

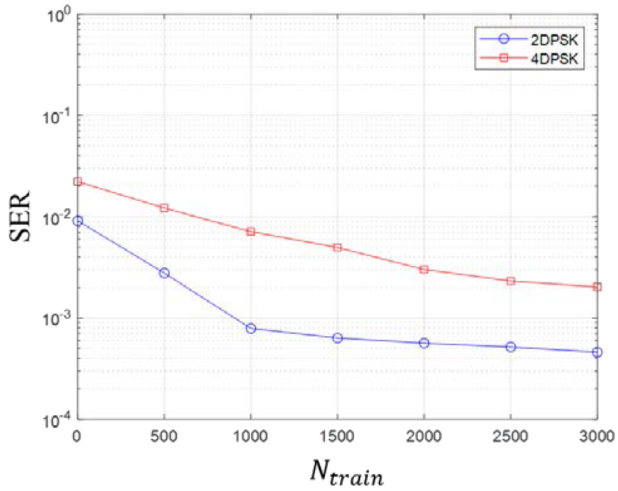

FIGURE 10. DPSK SER performance of the received 64QAM-PIR4FSK-Mary DPSK signal according to number of data symbol trainings.

This trend is also observed in Figure 9. Figure 9 shows the SER performance when a DPSK signal was received by 64QAM-PIR4FSK. The modulation order of the PIRFSK increased, and consequently, the overall SER performance decreased. However, the performance was improved through RNN equalization.

In addition, as shown in Figure 10, the DPSK SER performance of the received 64QAM-PIR4FSK–Mary DPSK signal at -3 dBm optical power was measured based on the number of total training symbols. The batch size is 50 and the iteration number is 5. 1 epoch is 250 data symbols trainings. Performance improvement as per the training was faster with 2DPSK than with 4DPSK. It was difficult to compensate for the degradation of the IDI generated as the number of DPSK levels increased. It was found that the effect on IDI increased as the number of levels of DPSK signals undergoing IDI increased, even under the same IDI generation

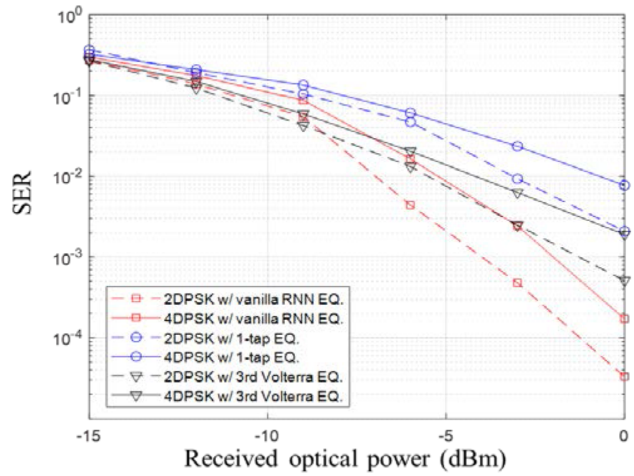

FIGURE 11. Total SER performance of the received 64QAM-PIR4FSK-Mary DPSK signal.

conditions. With the same intensity modulation, more training was required for IDI compensation as the modulation order of the DPSK signal increased. In this experiment, the RNN equalizer for the DPSK signal was trained 3,000 times, and the obtained SER values after equalization are shown in Figures 7–9.

Figure 11 shows the SER performance, including the QAM, PIRFSK, and DPSK signals. Figure 9 shows a similar trend in the performance, as shown in Figures 7–9. With 1-tap equalization and Volterra equalization, for 2DPSK, the QAM and PIRFSK signals were not affected by the IDI; therefore, SER performance deterioration did not occur; however, the DPSK signal significantly degraded the SER performance owing to the IDI of the IM signal. Similarly, the performance of 64QAM-PIR4FSK-4DPSK was determined by the DPSK with the lowest SER and the greatest IDI distortion. The SER performance after RNN equalization was similar to that shown in Figure 9. However, the SER of the QAM and PIRFSK, which were similar to those of the DPSK after IDI equalization, were combined to form cumulative SER. Finally, the total SER was slightly worsened. Through this performance improvement, it can be concluded that the IDI was effectively reduced.

We modulated and transmitted the proposed multi-dimensional optical signal simultaneously. After signal reception, the SER performance of the received signal was measured by performing IDI equalization through an RNN-based nonlinear equalization. When a multi-dimensional modulated signal is optically transmitted, IDI occurs and the transmission performance deteriorates. This performance degradation should be compensated, and we proved that RNN-based equalization is suitable for IDI-degradation compensation.

IV. CONCLUSION

We developed an IDI equalization technique for multi-dimensional modulation optical transmission using the QAM-PIRFSK-DPSK in a direct optical detection system. We conducted an RNN-based equalization for DPSK signal demodulation. The performance degradation of the DPSK signal caused by the IDI of the IM signal was analyzed while expanding the optical modulation dimensions. Using the proposed technique, it was verified that the RNN-based equalization was effective in reducing the interference between the modulation dimensions in QAM-PIRFSK-DPSK optical transmission. We experimentally demonstrated the performance of the proposed scheme. The results showed that the proposed equalization technique for the QAM-PIRFSK-DPSK system can be used to significantly increase the transmission capacity by utilizing a multi-dimensional optical transmission scheme.

REFERENCES

[1] A. Tzanakaki, M. Anastasopoulos, I. Berberana, D. Syrivelis, P. Flegkas, T. Korakis, and D. C. Mur, "Wireless-optical network convergence: Enabling the 5G architecture to support operational and end-user services," *IEEE Commun. Mag.*, vol. 55, no. 10, pp. 184–192, Oct. 2017.

[2] T. Pfeiffer, "Converged heterogeneous optical metro-access networks," in *Proc. 36th Eur. Conf. Exhib. Opt. Commun.*, Sep. 2010, pp. 1–6.

[3] C. Browning, A. Farhang, A. Saljoghei, N. Marchetti, V. Vujicic, L. E. Doyle, and L. P. Barry, "Converged wired and wireless services in next generation optical access networks," in *Proc. 19th Int. Conf. Transparent Opt. Netw. (ICTON)*, Jul. 2017, pp. 1–3.

[4] N. Cvijetic, "Next-generation optical access networks," *J. Lightw. Technol.*, vol. 25, no. 11, pp. 3428–3442, Nov. 1, 2007.

[5] J. Wang, M. K. Haldar, L. Li, and F. V. C. Mendis, "Enhancement of modulation bandwidth of laser diodes by injection locking," *IEEE Photon. Technol. Lett.*, vol. 8, no. 1, pp. 34–36, Jan. 1996.

[6] J. Cho, S. Chandrasekhar, G. Raybon, X. Chen, S. L. I. Olsson, and P. J. Winzer, "High spectral efficiency optical transmission with probabilistic constellation shaping," in *Proc. 23rd Opto-Electron. Commun. Conf. (OECC)*, Jul. 2018, pp. 1–2.

[7] J. Zhou, Y. Qiao, Z. Yang, and E. Sun, "Faster-than-Nyquist non-orthogonal frequency-division multiplexing based on fractional Hartley transform," *Opt. Lett.*, vol. 41, no. 19, p. 4488, 2016.

[8] T.-N. Duong, N. Genay, M. Ouzzif, J. Le Masson, B. Charbonnier, P. Chanclou, and J. C. Simon, "Adaptive loading algorithm implemented in AMOOFDM for NG-PON system integrating cost-effective and low-bandwidth optical devices," *IEEE Photon. Technol. Lett.*, vol. 21, no. 12, pp. 790–792, Jun. 2009.

[9] S. Zhang, F. Yaman, E. Mateo, T. Inoue, K. Nakamura, and Y. Inada, "A generalized pairwise optimization for designing multi-dimensional modulation formats," in *Proc. Opt. Fiber Commun. Conf. Exhib. (OFC)*, Mar. 2017, pp. 1–3.

[10] X. Zhou and J. Yu, "Multi-level, multi-dimensional coding for high-speed and high-spectral-efficiency optical transmission," *J. Lightw. Technol.*, vol. 27, no. 16, pp. 3641–3653, Aug. 2009.

[11] M. Karlsson and E. Agrell, "Multidimensional modulation and coding in optical transport," *J. Lightw. Technol.*, vol. 35, no. 4, pp. 876–884, Feb. 2017.

[12] S. Betti, P. Perrone, and G. G. Rutigliano, *Multidimensional Modulations in Optical Communication Systems*. Boca Raton, FL, USA: CRC Press, 2021.

[13] H. J. Park, I. H. Ha, S.-M. Kang, W.-H. Shin, and S.-K. Han, "3D QAM-DPSK optical transmission employing a single Mach–Zehnder modulator and optical direct detection," *J. Lightw. Technol.*, vol. 38, no. 22, pp. 6247–6256, Nov. 2020.

[14] I. Ha, J.-M. Lee, and S.-K. Han, "SOP change robust optical modulation based on dual polarization modulation for multi-dimensional optical transmission," *IEEE Access*, vol. 9, pp. 119139–119146, 2021.

[15] I. Ha, J. Lee, J. Park, and S.-K. Han, "Single wavelength simultaneous optical intensity-polarization-phase modulation for multi-dimensional optical transmission," *J. Lightw. Technol.*, vol. 40, no. 16, pp. 5605–5614, Aug. 2022.

[16] J. Lee, I. Ha, J. Park, and S.-K. Han, "Inter-signal distortion analysis in multidimensional QAM-MDPSK modulation optical access transmissions," *IEEE Access*, vol. 10, pp. 47266–47274, 2022.

[17] J. Park, I. Ha, J. Lee, and S.-K. Han, "Constellation shaped 3D HQAM-DPSK modulation for single wavelength multi-dimensional optical transmission," *IEEE Access*, vol. 11, pp. 22526–22530, 2023.

[18] J. Lee, I. Ha, J. Park, and S.-K. Han, "Inter-dimensional interference-tolerant 4-D set-partitioning QAM-MDPSK optical access network transmission," *Opt. Fiber Technol.*, vol. 78, Jul. 2023, Art. no. 103294.

[19] N.-P. Diamantopoulos, H. Nishi, W. Kobayashi, K. Takeda, T. Kakitsuka, and S. Matsuo, "On the complexity reduction of the second-order Volterra nonlinear equalizer for IM/DD systems," *J. Lightw. Technol.*, vol. 37, no. 4, pp. 1214–1224, Dec. 28, 2019.

[20] Y. Yu, M. R. Choi, T. Bo, Z. He, Y. Che, and H. Kim, "Low-complexity second-order Volterra equalizer for DML-based IM/DD transmission system," *J. Lightw. Technol.*, vol. 38, no. 7, pp. 1735–1746, Apr. 2020.

[21] J. Zhang, W. Chen, M. Gao, and G. Shen, "K-means-clustering-based fiber nonlinearity equalization techniques for 64-QAM coherent optical communication system," *Opt. Exp.*, vol. 25, no. 22, p. 27570, 2017.

[22] S. Liu, M. Xu, J. Wang, F. Lu, W. Zhang, H. Tian, and G.-K. Chang, "A multilevel artificial neural network nonlinear equalizer for millimeter-wave mobile fronthaul systems," *J. Lightw. Technol.*, vol. 35, no. 20, pp. 4406–4417, Oct. 2017.

[23] A. G. Reza and J. K. Rhee, "Nonlinear equalizer based on neural networks for PAM-4 signal transmission using DML," *IEEE Photon. Technol. Lett.*, vol. 30, no. 15, pp. 1416–1419, Aug. 2018.

[24] W.-H. Huang, H.-M. Nguyen, C.-W. Wang, M.-C. Chan, C.-C. Wei, J. Chen, H. Taga, and T. Tsuritani, "Nonlinear equalization based on artificial neural network in DML-based OFDM transmission systems," *J. Lightw. Technol.*, vol. 39, no. 1, pp. 73–82, Jan. 2021.

[25] S. Deligiannidis, C. Mesaritakis, and A. Bogris, "Performance and complexity analysis of bi-directional recurrent neural network models versus Volterra nonlinear equalizers in digital coherent systems," *J. Lightw. Technol.*, vol. 39, no. 18, pp. 5791–5798, Sep. 2021.

[26] Z. Xu, C. Sun, T. Ji, J. H. Manton, and W. Shieh, "Feedforward and recurrent neural network-based transfer learning for nonlinear equalization in short-reach optical links," *J. Lightw. Technol.*, vol. 39, no. 2, pp. 475–480, Jan. 2021.

[27] Q. Zhou, C. Yang, A. Liang, X. Zheng, and Z. Chen, "Low computationally complex recurrent neural network for high speed optical fiber transmission," *Opt. Commun.*, vol. 441, pp. 121–126, Jun. 2019.

INHO HA received the B.S. and M.S. degrees in electronic engineering from Yonsei University, Seoul, South Korea, in 2017 and 2019, respectively, where he is currently pursuing the Ph.D. degree in electrical and electronic engineering. His research interests include multidimensional optical transmission, wireless/wireline convergence, and next-generation mobile front haul.

JOUNG-MOON LEE received the B.S. degree in electrical and electronics engineering from Chung-Ang University, Seoul, South Korea, in 2020. He is currently pursuing the M.S. degree in electrical and electronic engineering with Yonsei University. His research interests include multidimensional optical transmission, OFDMA-PON, and next-generation access networks.

JINWOO PARK received the B.S. degree in electrical and electronics engineering from Yonsei University, Seoul, South Korea, in 2021, where she is currently pursuing the M.S. degree in electrical and electronic engineering. Her research interests include multi-dimensional optical transmission, OFDMA-PON, and next-generation access networks.

SANG-KOOK HAN (Senior Member, IEEE) received the B.S. degree in electronic engineering from Yonsei University, Seoul, South Korea, in 1986, and the M.S. and Ph.D. degrees in electrical engineering from the University of Florida, Gainesville, FL, USA, in 1994. From 1994 to 1996, he was with the System IC Laboratory, Hyundai Electronics, where he was involved in the development of optical devices for telecommunications. He is currently a Professor with the Department of Electrical and Electronic Engineering, Yonsei University. His current research interests include optical devices/systems for communications, optical OFDM transmission systems, optical networks, and optical wireless communications, including visible-light communication.